applied mechanics

MDPI

Article

Investigation of Mechanical Behavior and Damage Mechanisms in Synthetic and Bio-Based Sandwich Composites Using Acoustic Emission

Hana Driss [1,2,*], Abderrahim El Mahi [1], Mourad Bentahar [1], Moez Beyaoui [2] and Mohamed Haddar [2]

[1] Laboratoire d'Acoustique de l'Université du Mans (LAUM), UMR CNRS 6613, Institut d'Acoustique—Graduate School (IA—GS), CNRS, Le Mans Université, 72085 Le Mans, France; abderrahim.elmahi@univ-lemans.fr (A.E.M.); mourad.bentahar@univ-lemans.fr (M.B.)

[2] Laboratoire de Mécanique, Modélisation et Production (LA2MP), Ecole, Nationale d'Ingénieurs de Sfax (ENIS), Université de Sfax, Route de Soukra, Sfax 3038, Tunisia; moez.beyaoui@yahoo.fr (M.B.); mohamed.haddar@enis.tn (M.H.)

* Correspondence: hana.driss@enis.tn

Abstract

This paper presents the mechanical characterisation of sandwich composites. Different specimen configurations have been tested with a three-point bending load and their mechanical behavior has been discussed. In addition, the acoustic emission technique was used to detect the onset of damage mechanisms and to monitor their evolution. The proposed analysis is based on processing recorded acoustic emission bursts. An unsupervised classification approach, combining the k-means algorithm with Principal Component Analysis (PCA), is used to group the detected acoustic events. The cluster analysis of the acquired data allows for correlation with the damage mechanisms occurring in sandwich composites. In addition to the advantages of multivariate data analysis, the results highlight the influence of sensor placement on the analysis of damage mechanisms is investigated. A suitable sensor configuration is proposed to improve the detection of acoustic emission activity. The originality of this work lies in the combined mechanical–AE interpretation that provides new insight into the damage behaviour of both a synthetic and a bio-based sandwich material. The comparative analysis of these two types of materials, coupled with a dedicated evaluation of sensor placement effects on defect detection, offers a contribution not previously reported in the literature.

Keywords: acoustic emission; damage mechanics; sandwich composite; mechanical properties

check for updates

Received: 5 November 2025
Revised: 5 December 2025
Accepted: 8 December 2025
Published: 12 December 2025

Citation: Driss, H.; El Mahi, A.; Bentahar, M.; Beyaoui, M.; Haddar, M. Investigation of Mechanical Behavior and Damage Mechanisms in Synthetic and Bio-Based Sandwich Composites Using Acoustic Emission. *Appl. Mech.* **2025**, *6*, 90. https://doi.org/10.3390/applmech6040090

Copyright: © 2025 by the authors. Licensee MDPI, Basel, Switzerland. This article is an open access article distributed under the terms and conditions of the Creative Commons Attribution (CC BY) license (https://creativecommons.org/licenses/by/4.0/).

1. Introduction

The design of structures with a lightweight core between two composite skins aims to increase stiffness and flexural strength properties with minimal impact on overall mass. It is therefore essential to improve our understanding of the relationships between loads, material properties and damage in composite sandwich materials. The level of understanding must be advanced so that the complex damage processes that occur in sandwich structures can be accurately monitored and predicted. Studies have analyzed shear cracking in foam-core sandwich panels and emphasized its effect on strength. Zenkert and Vikstrom [1] used infrared imaging and fracture mechanics to detect and analyze these cracks and showed that their presence significantly reduces the strength of sandwich beams. These cracks, which result from overload or fatigue, occur primarily in the center plane of the core before

propagating [2]. Nordstrand and Carlsson [3] evaluated the transverse shear stiffness of corrugated core sandwich panels using three-point bending tests and found a lower shear modulus than those obtained using block shear due to local indentation effects. Daniel and Jandro [4] studied bending of composite sandwich beams and found premature failure due to shear crimping of the core.

In recent years, further progress has been made in applying hybrid nondestructive evaluation (NDT) techniques to sandwich composites. For example, low-velocity impact damage has been quantitatively assessed in sandwich panels using a combined pulsed thermography and ultrasonic phased-array approach, providing accurate mapping of internal delaminations and impact zones [5]. In addition, terahertz time-domain spectroscopy (THz-TDS) has been successfully applied to detect internal defects such as debonding, pores, and cracks in thicker foam-core sandwich panels, offering a non-contact, high-resolution imaging alternative [6]. On another front, guided ultrasonic wave methods have advanced considerably: recent reviews highlight the integration of piezoelectric sensors, advanced signal processing, and machine-learning algorithms to improve damage detection, localization, and classification in composite structures [7]. These emerging techniques strengthen the case for a multimodal NDT/SHM strategy in sandwich structures, enabling earlier, more reliable detection of damage and therefore more effective prediction of failure.

Given these challenges, recent studies have demonstrated the effectiveness of infrared thermography for detecting internal damage in honeycomb sandwich composites, providing a non-destructive method to assess the structural integrity of these materials [8]. Additionally, the integration of machine learning techniques in the analysis of AE signals has significantly enhanced the detection and classification of damage mechanisms in composite structures, leading to improved real-time structural health monitoring [9]. Furthermore, advanced numerical modeling approaches have been developed to predict the progressive failure of sandwich structures, allowing better anticipation of damage evolution under various loading conditions [10].

Non-destructive testing methods such as ultrasonic testing [11,12] and acoustic emission testing have been widely used to study damage mechanisms in composite materials [13,14]. The changes generate measurable mechanical energy that propagates as an acoustic wave. Piezoelectric sensors placed on the surface of the material detect the elastic waves in the form of Acoustic Emission (AE) signals on the specimen. These can be characterized by various parameters such as amplitude, energy, rise time, and duration [15,16]. The temporal and frequency parameters of AE signals are used to study damage in glass or carbon fiber composites [17–20]. Various AE signal classification methods are used to associate acoustic events with degradation mechanisms. Consequently, this technique can be used to monitor the evolution of specific defects in real time, such as integrated structural health monitoring (SHM) [21]. Moreover, the influence of environmental conditions, such as temperature and humidity, on the acoustic properties of composite materials has been investigated, revealing significant variations in AE signal characteristics under extreme conditions [22].

Finally, an in-depth understanding of composite degradation mechanisms remains essential to fine-tune damage detection and prevention methods. Numerous studies have been conducted on composites and fibers to characterize their degradation mechanisms [23]. For example, Rhomany et al. [24] used AE to monitor a tensile test performed on a flax fiber. Based on the amplitude of the recorded signals, they were able to distinguish between events corresponding to longitudinal separation of elementary fibers, transverse fiber cracks, and complete fiber breakage. Other researchers have performed tests on pure matrix samples to characterize degradation mechanisms, such as matrix cracking or matrix/matrix friction [25]. At the composite scale, the most commonly studied degradation mechanisms

are matrix cracking, fiber/matrix interface delamination, and fiber breakage. Numerous multiparameter studies have highlighted the importance of the amplitude of AE signals. For example, amplitudes between 40 and 60 dB are commonly associated with matrix cracking, while fiber/matrix interface decohesion is often correlated with signals with amplitudes between 45 and 70 dB [26]. It should be noted that the values of these intervals depend on the type of reinforcement and matrix considered. Table 1 summarizes the main acoustic properties in terms of amplitude of damage mechanisms created within different composites [21,22]. The amplitude ranges listed in Table 1 are used only as qualitative guidance. Because AE amplitudes depend strongly on the material system, specimen geometry, sensor placement, and acquisition settings, these values cannot be applied as strict thresholds. In this work, AE events are classified solely through an unsupervised, data-driven clustering approach, and the Table 1 ranges are used only to support the post-interpretation of the resulting clusters.

Recent studies have applied AE monitoring specifically to sandwich and bio-based composites under flexural or impact loading. For example, low-velocity impact damage in foam-core sandwich panels has been characterized using AE combined with optical scanning and X-ray computed tomography, enabling correlation of AE signals with internal delaminations and damage zones [27]. AE has also been used during bending of nanotube/nanocellulose-reinforced foam-core sandwiches to detect core damage and face-sheet/core debonding [28]. Bio-based sandwich structures with balsa wood cores have been investigated to assess how moisture content affects AE characteristics and damage evolution under flexural loading [29]. Additionally, AE combined with digital image correlation has been applied to localize failure zones in sandwich beams, improving the interpretation of AE events [30]. While these studies have advanced AE applications in sandwich structures, systematic classification of AE signals and the effect of sensor placement remain insufficiently addressed, and direct comparisons between synthetic and bio-based cores under bending are scarce. The present work extends these investigations by applying unsupervised clustering to AE data during three-point bending, systematically evaluating sensor-location effects, and correlating AE signal classes with observed failure modes, thereby providing a more robust framework for AE-based structural health monitoring of sandwich composites.

Although several previous studies have already applied acoustic emission monitoring to sandwich composites, this work introduces new elements. In this study, the combination of three-point static bending tests with an unsupervised clustering strategy provides a clearer and more consistent correlation between AE signal classes and failure modes observed experimentally in foam-core sandwich beams. Furthermore, unlike our previous AE research, the influence of sensor placement on AE activity detection and interpretation is systematically evaluated in order to improve the reliability of AE-based damage identification in sandwich structures.

In summary, previous research has provided valuable insights into damage mechanisms in sandwich composites and has demonstrated the usefulness of AE for monitoring matrix cracking, interface debonding, and fiber fracture. However, existing studies rarely establish a clear and systematic correlation between AE signal classes and experimentally observed failure modes in foam-core sandwich beams. In addition, the influence of sensor placement on AE detection sensitivity and damage interpretation remains insufficiently explored, even though it is critical for reliable SHM implementation. The present work addresses these gaps by combining three-point static bending tests with an unsupervised clustering strategy and by evaluating, for the first time in a systematic manner, how different sensor locations affect the detection and classification of AE activity. This approach provides a more robust framework for interpreting AE signatures in sandwich structures.

For sandwich structures, the development and progression of failure modes are complex due to the simultaneous presence of multiple constituents. The initiation, propagation, and interaction of damage mechanisms depend on material properties, geometry, constituent characteristics, and the type of applied load. To ensure reliable detection of the acoustic waves generated by these damage mechanisms, three piezoelectric sensors are placed on the top and bottom skins as well as within the core according to standard acoustic emission practice.

This article presents an experimental and analytical study of the behavior of sandwich beams in static bending. The study then focuses on an unsupervised classification approach, grouping events into signal classes according to their similarities. Furthermore, additional mechanical investigations are conducted to establish correlations between the observed damage mechanisms and the various signal classes. The objective of this study is to provide an insight into the underlying reasons for the static behavior of the sandwich and its components.

Table 1. Acoustic properties of the main damage mechanisms for the two types of composites.

Damage	Material	Characteristics	Reference
Matrix cracking	Flax/Epoxy	Amplitude [42–60] dB	[31]
	Glass/Epoxy	Amplitude [45–60] dB Amplitude [~50–70] dB	[32–35]
Decohesion Fiber/matrix	Flax/Epoxy	Amplitude [60–70] dB	[31]
	Glass/Epoxy	Amplitude [60–80] dB Amplitude [~55–80] dB	[32–35]
Interfacial delamination	Flax/Epoxy	Amplitude [48–65] dB	[36]
	Glass/Epoxy	Amplitude [60–80] dB Amplitude [~55–70] dB	[32–35]
Fiber breakage	Flax/Epoxy	Amplitude [70–100] dB	[31]
	Glass/Epoxy	Amplitude [80–90] dB Amplitude [~70–100] dB	[32–35]

2. Materials and Methods

2.1. Materials

In the present study, a range of cores were selected as the fundamental components of the composite materials under investigation. Balsa and PVC foams were selected for this primary function. The outer layers of the composites were formed by incorporating glass and flax fibres with surface densities of 202 g/m^2 and 115 g/m^2, respectively. The flax fibres were dried at 110 °C for one hour in a ventilated oven [30]. This procedure is widely regarded as the most effective method for removing excess moisture without compromising the mechanical properties of the fibres. Epoxy (SR-5600, Gurit, Switzerland) and GreenPoxy resin (SR GreenPoxy 56) were thoroughly impregnated. The thickness of the cores and outer layers of all the samples was standardised to ensure uniform experimental conditions. A study was conducted to investigate the impact of core density and composition on the mechanical properties of sandwich structures. To this end, three distinct types of cores were deliberately selected for analysis. The first type of core, with an average density of 60 kg/m^3, is composed of PVC, thus representing a synthetic core. The second type, also made of PVC, has a density of 80 kg/m^3. In addition, a third type of core was included in the investigative approach, which was of bio-sourced origin (balsa) and had a density of 150 kg/m^3.

The materials will be designated as follows:

[FF_4/$Balsa_{150}$/FF_4]: 'FF' represents the Flax Fabric, 'FF_4' indicates that four plies of Flax are superimposed, and '$Balsa_{150}$' designates the core of the composite, made of Balsa with a density of 150 kg/m^3.

[GF_2/PVC_{60}/GF_2]: 'GF' represents the Glass Fabric, 'GF_2' indicates that two plies of glass fabric are superimposed, and 'PVC_{60}' designates the core of the composite, made of PVC with a density of 60 kg/m^3.

[GF_2/PVC_{80}/GF_2]: The nomenclature remains consistent, with the exception of the core density. In this case, 'PVC_{80}' denotes a PVC core with a density of 80 kg/m^3.

Table 2 summarizes the three sandwich configurations and the rationale for their selection. The two synthetic sandwiches [GF_2/PVC_{60}/GF_2] and [GF_2/PVC_{60}/GF_2] allow studying the effect of core density while keeping skins identical. The bio-based sandwich [FF_4/$Balsa_{150}$/FF_4] enables comparison with a fully sustainable structure and assessment of natural fibers and cores versus synthetic counterparts.

Table 2. Summary of the tested sandwich configurations and justification for their selection.

Designation	Reason for Using This Configuration
[FF_4/$Balsa_{150}$/FF_4]	• To evaluate a bio-based alternative to synthetic sandwiches. • To assess the effect of a high-density natural core on stiffness, damage evolution, and AE activity. • To compare bio-based skins (flax) with synthetic skins (glass). • To study the potential of sustainable sandwich structures for real applications.
[GF_2/PVC_{60}/GF_2]	• Acts as an industrial baseline representing lightweight marine/automotive sandwich panels. • Allows isolating the effect of low core density on bending response and failure modes. • Provides reference AE signatures for lightweight synthetic cores. • Enables comparison with the higher-density PVC_{80} core while keeping skins identical.
[GF_2/PVC_{80}/GF_2]	• Enables a controlled study of core-density influence (60 vs. 80 kg/m^3) with identical skins. • To analyze how higher density affects load capacity, failure initiation, and AE signal classes. • Allows direct comparison with the bio-based balsa core under similar bending conditions. • Represents a stiffer synthetic configuration used in structural applications requiring higher strength.

In the fabrication of the sandwich samples, a total of 4 or 8 plies of fabric are utilised for the top and bottom skins, respectively, composed of glass and flax. The epoxy/hardener mixture is prepared in a ratio of 3:1. The manufacturing process commences with the preparation of the mould. Subsequently, the layers of fabric are impregnated with resin. Subsequent to the laying down of the glass or Flax plies, a PVC or balsa board is positioned on an evenly distributed layer of resin. On the opposing side of the core, an equivalent number of glass or Flax plies are applied. Figure 1 provides a representative diagram of an assembly made up of glass fibres for the skins and a PVC foam core.

The assembly is meticulously wrapped in standard plastic film and subjected to a vacuum process at a pressure of 300 mbar for a duration of 10 h. It is important to note that no pressure is exerted on the mould during the vacuum process. Subsequent to the completion of the vacuum process, which is a period of 10 h, the vacuum pump is deactivated and the sheet is extracted from the vacuum chamber. The plates are then cut into samples using a diamond disk cutter. The specimens utilised for the bending tests are precisely 300 mm in length, 25 mm in width, and possess a nominal thickness of 8 mm.

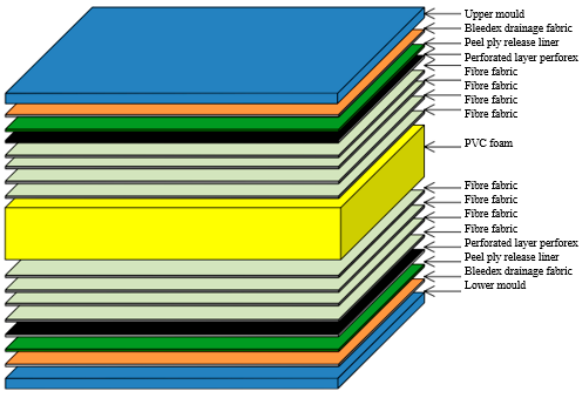

Figure 1. Sandwich composite assembly diagram.

2.2. Experimental Setup

2.2.1. Mechanical Method

The bending tests were conducted in accordance with the standard NF T 54-606 [37]. This standard defines the procedure for bending tests on polymer and composite materials and ensures repeatable and comparable results, which makes it suitable for the materials tested in this study. The test consists of applying a load P to the beam, which is supported on two points spaced at a distance d, causing a displacement W. The load can be applied at a single point (or on a single line) at the centre of the two supports, thus constituting three-point bending. The selection of test type and the distance between supports is contingent on the properties to be studied. A configuration of distant supports will favour pure bending of the beam, while closer supports will favour shearing. For the purposes of this study, an Instron 8801 universal tension/compression machine (Instron, Norwood, MA, USA) equipped with a 10 kN Instron load cell was used in conjunction with the three-point bending device depicted in Figure 2. The machine was fitted with an anti-rotation device to prevent rotation of the lower supports around the axis of the hydraulic cylinder, particularly during cyclic testing.

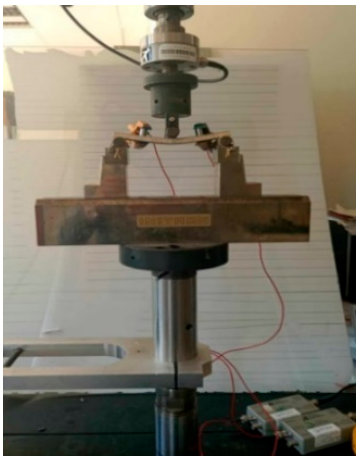

Figure 2. Three-point bending tests were performed on sandwich beams in accordance with the NF T 54-606 standard, with acoustic emission monitoring.

Various sandwich beam configurations were tested under three-point bending until failure, using a span length *d* of 250 mm and a central roller with a diameter of 20 mm. The load was applied at a displacement rate of 1 mm/min during the bending tests. The choice of a 250 mm span allowed all specimens to retain the same overall length for both bending and shear tests, with only the support spacing being adjusted between configurations. This span length also complies with the recommendations of the relevant standards. A crosshead

displacement rate of 1 mm/min was applied to ensure quasi-static loading conditions. Acoustic emission was employed to track failure modes and damage mechanisms in the sandwich materials. Quasi-static bending tests were conducted on all samples to analyze the key characteristics of each sandwich structure.

Further bending-to-failure tests were carried out on beams with different distances between supports, to subject them to pure bending (where distances between supports are longest) and shear (where distances between supports are shortest). The specimens examined were all 25 mm wide and d + 50 mm long, with d representing the distance between supports. Three to five specimens were tested per test and per material.

To ensure the reliability of the mechanical measurements, each bending configuration was tested on three to five specimens, and the repeatability of the results was quantified. The measurement uncertainty was evaluated from the standard deviation and coefficient of variation of the maximum load, displacement at failure, and stiffness obtained across repeated tests. In addition, the precision of the 10 kN load cell (±0.5%) and the displacement transducer (±0.02 mm) were taken into account when estimating the global uncertainty. This approach ensures that the variability reported in the results reflects both material heterogeneity and the intrinsic accuracy of the testing system.

2.2.2. Acoustic Emission Method

Two broadband piezoelectric transducers from Physical Acoustics (frequency range 100 kHz–1 MHz) were utilised, as illustrated in Figure 3. Acoustic events were recorded in real time at an acquisition frequency of 5 MHz. Preliminary tests set the detection threshold at 38 dB.

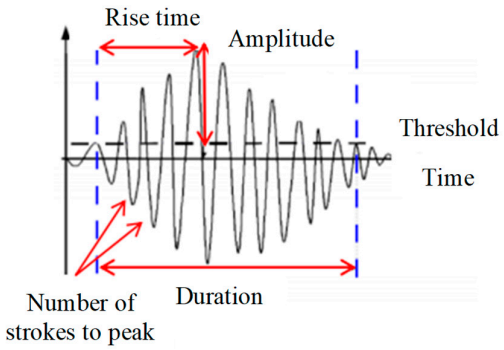

Figure 3. Establishing temporal criteria for classifying AE signals.

In addition, in order to optimise the detection of AE signals, the following measures were applied: HDT = 100 µs, PDT = 50 µs, and HLT = 200 µs. An acquisition threshold of 38 dB was selected based on preliminary noise measurements, ensuring that background and mechanical noise remained below the detection limit while maintaining sensitivity to low-amplitude AE events. Finally, two 40 dB preamplifiers were used and all the acquisitions were made using AE-Win software (version 3.20, Physical Acoustics, Princeton Junction, NJ, USA). Depending on the specimen and its damage evolution, each sensor typically recorded between a few hundred and several thousand AE hits during a single bending test.

Following the tests, the acoustic emission data were analysed using NOESIS software (version 4.4, Envigilant Systems, Toulouse, France) and a customised procedure using MATLAB software (version 2018b, MathWorks, Natick, MA, USA). The five selected temporal parameters include rise time, duration, amplitude, signal energy, and the number of peaks (see Figure 3 [32]).

For unsupervised classification, the k-means algorithm is used [38]. This algorithm aims to divide a population of n events into an optimal number of k classes. Each event is

associated with the class with the most similar average properties. To facilitate comparison, we first normalised the data by centring and reducing it. This normalisation was applied to all the signals as described by Equation (1).

$$\forall i \in \Omega_p, p \in \Delta : z_i = \frac{x_i - m_{x_p}}{\sigma_{x_p}} \quad (1)$$

In this equation, each term x_i represents an individual event in the dataset Ω_p, which is associated with classifier p. The values m_{x_p} et σ_{x_p} correspond to the mean and standard deviation, respectively, of the dataset Ωp, while Δ represents the set of selected classifiers.

To initiate the k-means process, we opted for an initial random partitioning and used the Euclidean distance as the dissimilarity metric [38,39]. We then ran the algorithm iteratively (1000 iterations), varying the number of classes from 2 to 7. At each stage of this procedure, we calculated the Davies and Bouldin coefficient [39], the minimisation of which allows us to find the optimal number of classes:

$$R_{ij}(D\&B) = \frac{1}{k}\sum_{i=1}^{n} max_i \left(\frac{d_i + d_j}{d_{ij}}\right) \quad (2)$$

K represents the number of classes, where d_i and d_j denote the mean intra-class distances, and d_{ij} corresponds to the mean inter-class distance.

3. Results and Discussion

3.1. Behavior of Sandwich Materials

3.1.1. Static Bending Behavior

Figure 4 shows the evolution of load as a function of displacement for the different sandwich materials. In the curve in Figure 4a, the elastic behavior is quasi-linear up to the maximum load, which is of the order of 175 N for the sandwich [$GF_2/PVC_{60}/GF_2$] and 210 N for [$GF_2/PVC_{80}/GF_2$]. Thereafter, the behavior becomes non-linear up to the maximum load. Thereafter, the load decreases with increasing displacement until failure. The behavior of the synthetic sandwich is divided into three distinct regions.

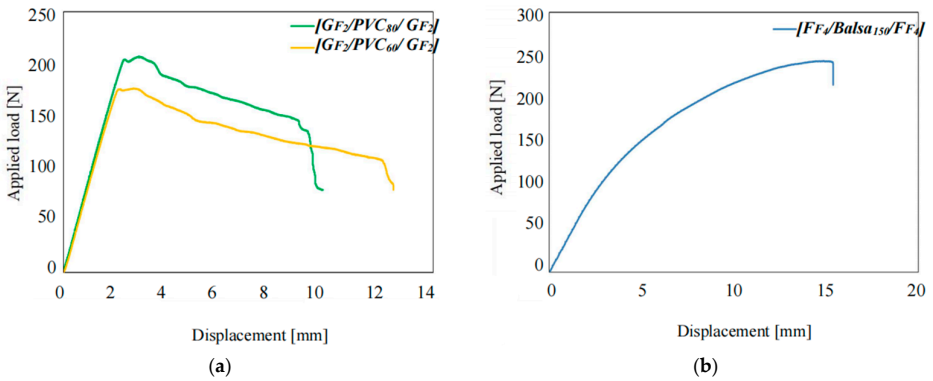

Figure 4. Evolution of load as a function of displacement for different sandwiches: (**a**) synthetic and (**b**) bio-sourced.

The initial region primarily reflects the compressive response of the upper skin laminate, characterized by a reversible linear behavior. In this phase, transverse cracking begins, progresses, and develops within the laminate.

The second region represents the compressive behavior of the core due to bending of the upper skin, leading to a non-linear evolution of the load-displacement curve depending mainly on the properties of the core. The duration of this phase is influenced by the

characteristics of the core, being shorter for the sandwich with a core density of 80 kg/m^3. An increase in core density results in an increase in the ultimate load and greater stiffness of sandwich materials.

In the third phase, as the load increases, decohesion between the skin and the core initiates and progresses, ultimately causing skin rupture. Once the skin fails, the load is redistributed to the core, which undergoes localized crushing. The core experiences compressive stresses, manifested by an extended region with a decreasing curvature. As this phase concludes, the various failure mechanisms interact, culminating in the complete failure of the specimen.

Several observations can be made by comparing these results. Firstly, the [GF_2/PVC_{60}/GF_2] and [GF_2/PVC_{80}/GF_2] configurations appear stiffer than the [FG_4/$Balsa_{150}$/FG_4] sandwich, due to the glass fabric skins, which therefore have a higher modulus than the flax fiber fabric. For sandwiches with glass skins, the linear elastic range appears to be more pronounced than for the sandwich with flax skins.

The mean values for stiffness, maximum load and displacement at break of the statically tested specimens are shown in Table 3.

Table 3. Average properties of statically tested sandwich specimens.

Sandwiches	Stiffness [N mm^{-1}]	Maximum Force [N]	Breaking Displacement [mm]	Number of Samples
[GF_2/PVC_{60}/GF_2]	78 ± 2	176 ± 4	12.2 ± 0.3	4
[GF_2/PVC_{80}/GF_2]	84 ± 2	207 ± 5	9.5 ± 0.25	4
[FF_4/$Balsa_{150}$/FF_4]	38 ± 1	244 ± 6	15.4 ± 0.4	4

These data clearly show that the value of the load depends strongly on the density of the sandwich core. As the core density increases, the breaking load increases. The higher displacement at break for [FF_4/$Balsa_{150}$/FF_4] indicates a better ability of the composite to resist high loads while maintaining its structural integrity. This can be attributed in part to the nature of the materials. The higher density of the balsa core also contributes to the overall strength of the sandwich. The larger area under the force-displacement curve [FF_4/$Balsa_{150}$/FF_4] suggests a greater capacity for energy absorption (approximately 1.9 J) and deformation prior to failure. This can be useful in situations where the structure needs to absorb large loads without suffering premature failure.

3.1.2. Equivalent Stiffnesses

In this section, the results of the bending tests were used to determine the elastic properties of the sandwiches and their components (skins and core). To achieve this objective, the three previous sandwiches were subjected to bending tests to determine the equivalent bending and shear stiffnesses. Some of these parameters were extracted using sandwich beam theory and drawing on previous work [40]. It is then possible to deduce the Young's modulus of the skins and the shear modulus of the cores.

In 3-point bending, the relationship between the measured deflection W and the applied load P is determined for a distance between supports d by:

$$\frac{W}{P} = \frac{d^3}{48D} + \frac{d}{4N} \tag{3}$$

For 4-point bending, a similar relationship is established, where the deflection/load ratio W_1/P_1 for a distance between supports d_1 is given by:

$$\frac{W_1}{P_1} = \frac{d_1^3}{768D} + \frac{d_1}{8N} \tag{4}$$

It should be noted that these deflection/load ratios depend on the equivalent bending stiffnesses D and shear stiffness N. At least two experimental methods can be used to determine the equivalent stiffnesses D and N, each involving variation of the test boundary conditions. Since Equations (3) and (4) form a system of two equations with two unknowns, the results of both 3-point and 4-point bending tests can be used. Therefore, the equivalent stiffnesses are obtained as follows:

$$D = \frac{Pd^3\left(1 - \left(\frac{11d_1^2}{8d^2}\right)\right)}{48W\left(1 - \left(\frac{2PdW_1}{P_1d_1W}\right)\right)} \tag{5}$$

$$N = \frac{Pd\left(\frac{8d^2}{11d_1^2} - 1\right)}{4W\left(\frac{16Pd^3W_1}{11P_1d_1^3W} - 1\right)} \tag{6}$$

Another method shows that with a specific type of test, such as 3-point bending, Equation (3) can be expressed as follows:

$$\frac{W}{Pd} = \frac{d^2}{48D} + \frac{1}{4N} \tag{7}$$

The method consists of testing sandwich beams in bending by varying the distance d between the supports. Figure 5 shows the evolution of the $W/(Pd)$ ratios as a function of d^2. The experimental points can be interpolated by a straight line. Using Equation (7), the slopes and y-intercepts of these lines can be used to determine the equivalent flexural and shear stiffnesses for the three sandwiches.

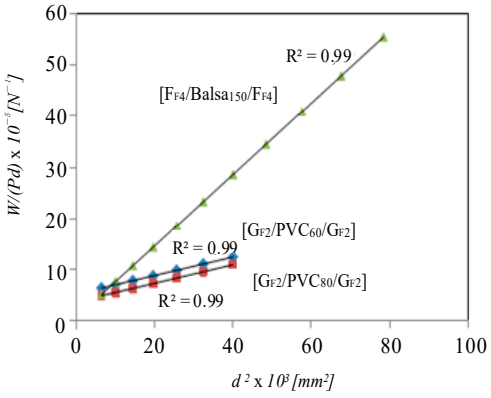

Figure 5. Evolution of the *W/(Pd)* ratio as a function of the square of the distance between supports for the three sandwiches.

Table 4 shows the equivalent stiffnesses measured. Due to the nature of the different skin fibres between the synthetic and bio-based sandwiches, the equivalent flexural stiffnesses differ. However, the values of the equivalent shear stiffnesses vary for the three materials because they depend mainly on the shear properties of the core.

Table 4. Measured elastic properties of the three sandwiches.

Sandwiches	$D.10^5$ [N/mm^2]	N [kN]
[$GF_2/PVC_{60}/GF_2$]	116 ± 6	4.8 ± 0.3
[$GF_2/PVC_{80}/GF_2$]	116 ± 6	6.8 ± 0.4
[$FF_4/Balsa_{150}/FF_4$]	30 ± 1.5	40 ± 2

Based on the previous findings, it is possible to deduce the main properties of the components of sandwich beams from the values of the equivalent stiffnesses D and N. Using the equations derived from the assumption of a core with limited mechanical properties, the Young's modulus of the composite skin, denoted Ep, can be obtained by:

$$E_p = \frac{2D}{be_p d^2} \tag{8}$$

where e_p is the thickness of the skin and b its width.

In addition, assuming thin skins and a core with low mechanical strength, the equivalent shear stiffness N of a sandwich beam can be defined, as a function of, in particular, the shear modulus G_a of the core, in accordance with the following expression:

$$G_a = \frac{Ne_a}{bd^2} \tag{9}$$

where e_a is the core thickness and $d = e_a + e_p$

The results obtained are shown in Figures 6 and 7.

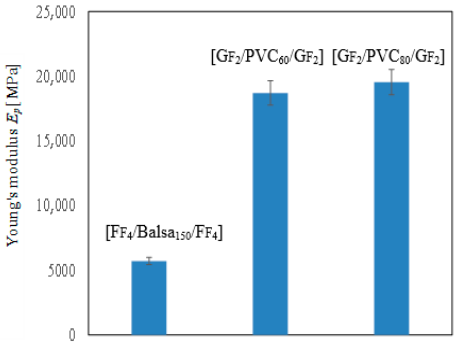

Figure 6. Illustration of the Young's modulus of the skins for different sandwiches.

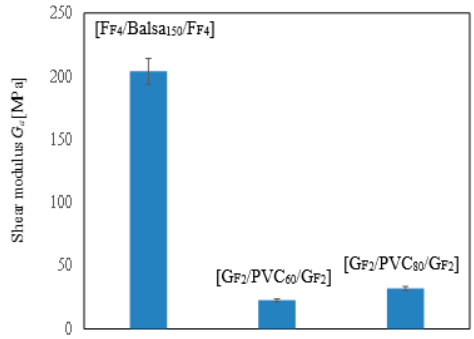

Figure 7. Illustration of core shear modulus for different sandwiches.

3.2. Assessment of Damage Mechanisms Using Acoustic Emission

This section presents the analysis of acoustic emission signals recorded during mechanical testing. The key features of the AE signals, such as amplitude, energy, duration, rise time, and the number of cycles to peak, are used to establish a classification method for these signals. Given the complexity of sandwich structures and the uncertainty surrounding the number of failure mechanisms at play, an unsupervised pattern recognition approach was employed. This approach was further enhanced by principal component analysis to improve the classification of the recorded AE signals. The goal of this study is to identify the failure mechanisms and track their progression over time, both independently and in combination, up until material rupture occurs.

In sandwich structures, the creation and progression of various failure modes are complicated by the coexistence of different materials. The development, spread, and interaction of damage mechanisms are influenced by the properties of the materials, their geometries, their constituents, and the applied load conditions. To enhance the detection of acoustic waves emitted by damage mechanisms in the sandwich structure, three piezoelectric sensors are strategically positioned on both the upper and lower faces, as well as within the core. More specifically, the sensors attached to the top and bottom sheets are positioned halfway across the width and halfway between the supports and the load roller, in order to avoid edge effects and minimize signal interference caused by contact between the load cylinder and the beam. On the core, the sensors are positioned halfway through the thickness and centered along the length of the beam. This symmetrical configuration ensures uniform wave detection and reduces location bias.

3.2.1. Synthetic Sandwiches

The results of acoustic activity in synthetic sandwich structures are displayed in Figure 8. These results highlight the crucial influence of sensor positioning on capturing acoustic emission (AE) signals in sandwich composites. Sensors placed on the top and bottom skins record significantly higher AE activity than those located within the core. Understanding the origin of ultrasonic waves generated by failure mechanisms requires considering the acoustic impedances of the various components.

When positioned on the skins, sensors likely detect acoustic waves from both the skins and the core, as illustrated in Figure 8a,b. However, due to differences in acoustic impedance, a significant portion of the elastic wave energy is reflected at the skin-core interface. As a result, the contribution of core damage to the signals captured by these sensors is primarily associated with damage occurring at the interface. These waves, originating from the interfaces, are unlikely to be detected by the sensor positioned on the core due to significant scattering and attenuation in the PVC foam. This explains why no failure mechanisms, apart from core cracking, are detected in the signals from the sensors placed on the foam, as seen in Figure 8c.

Therefore, mechanisms marked as 'not detected' do not imply that the damage is absent rather, their acoustic signatures fall below the detection capability of the core sensor because of strong wave attenuation within the PVC foam.

Figure 9 displays the results of the signal classification. It shows, using a semi-logarithmic scale, the progression of the number of acoustic events recorded during the bending test. Based on the AE parameters (rise time, duration, amplitude, signal energy, and the number of peaks), it is evident that the matrix cracking mechanism begins at the onset of the flexure test. This mechanism represents 64.3% of the total damage, that is, the complete set of acoustic emission (AE) events recorded for the specimen corresponding to the sum of all identified damage mechanisms occurring in the upper skin, lower skin, and the core for [$GF_2/PVC_{60}/GF_2$], and 60% for [$GF_2/PVC_{80}/GF_2$]. For the former sandwich, 56.8% of these events originate from the upper skin compared to 7.5% from the lower skin, while for the latter configuration, 53% of the events are associated with the upper skin versus 7% with the lower skin.

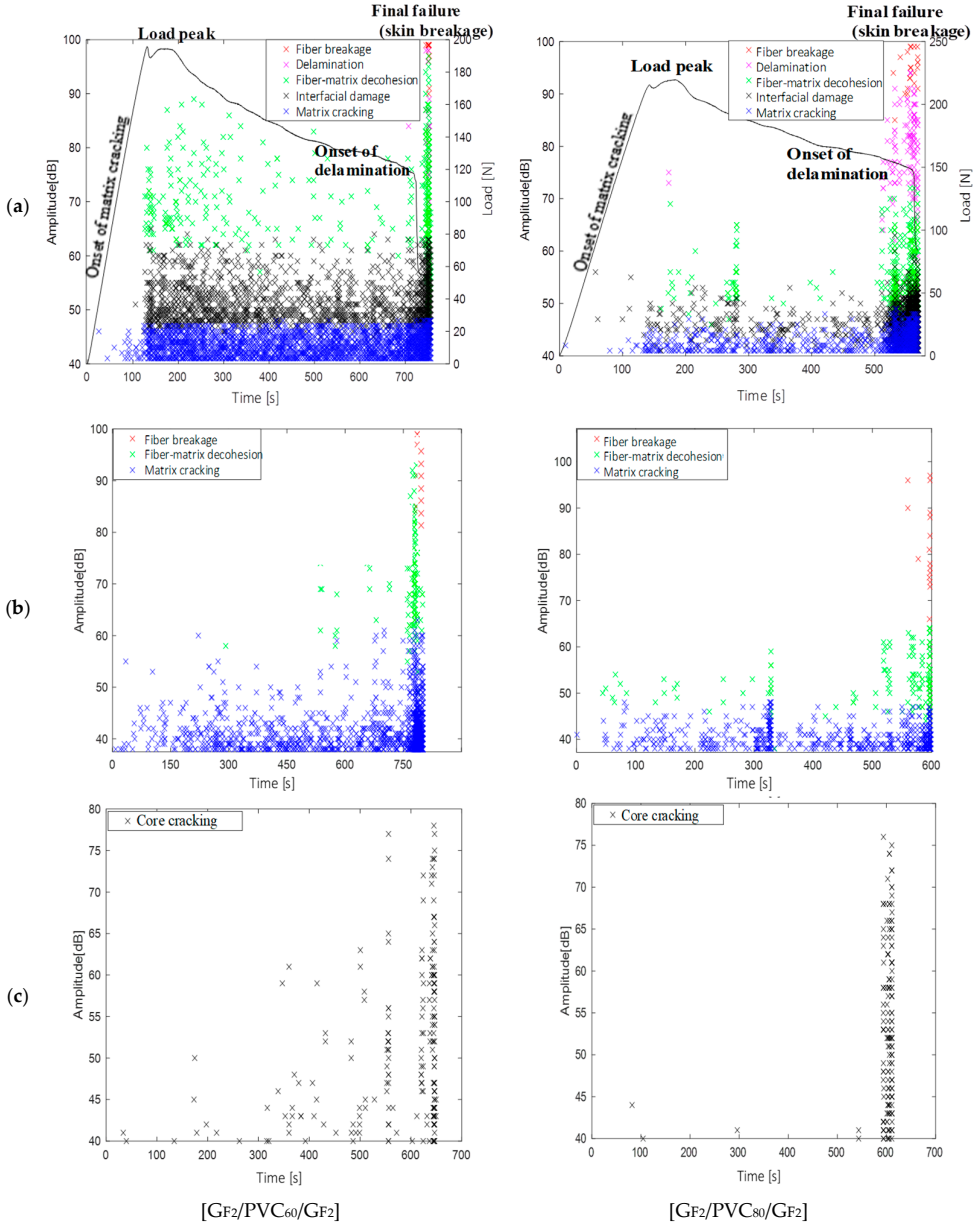

Figure 8. AE signal amplitudes as a function of bending test time for $[GF_2/PVC_{60}/GF_2]$ and $[GF_2/PVC_{80}/GF_2]$ sandwiches for a sensor placed on: (**a**) top skin, (**b**) bottom skin and (**c**) core.

This mechanism is followed by fiber and matrix delamination, which accounts for 4.1% in the top skin and 0.7% in the bottom skin for $[GF_2/PVC_{60}/GF_2]$, while for $[GF_2/PVC_{80}/GF_2]$ it is 7.6% in the top skin and 1.4% in the bottom skin. When these two events occur on both skins, only the top skin sensor can detect skin delamination and interfacial delamination between the PVC core and the skin. They account for only 0.4% and 29.3% of the overall damage for pour $[GF_2/PVC_{60}/GF_2]$, respectively. For $[GF_2/PVC_{80}/GF_2]$, they account for only 1.3% and 28% of overall damage, respectively.

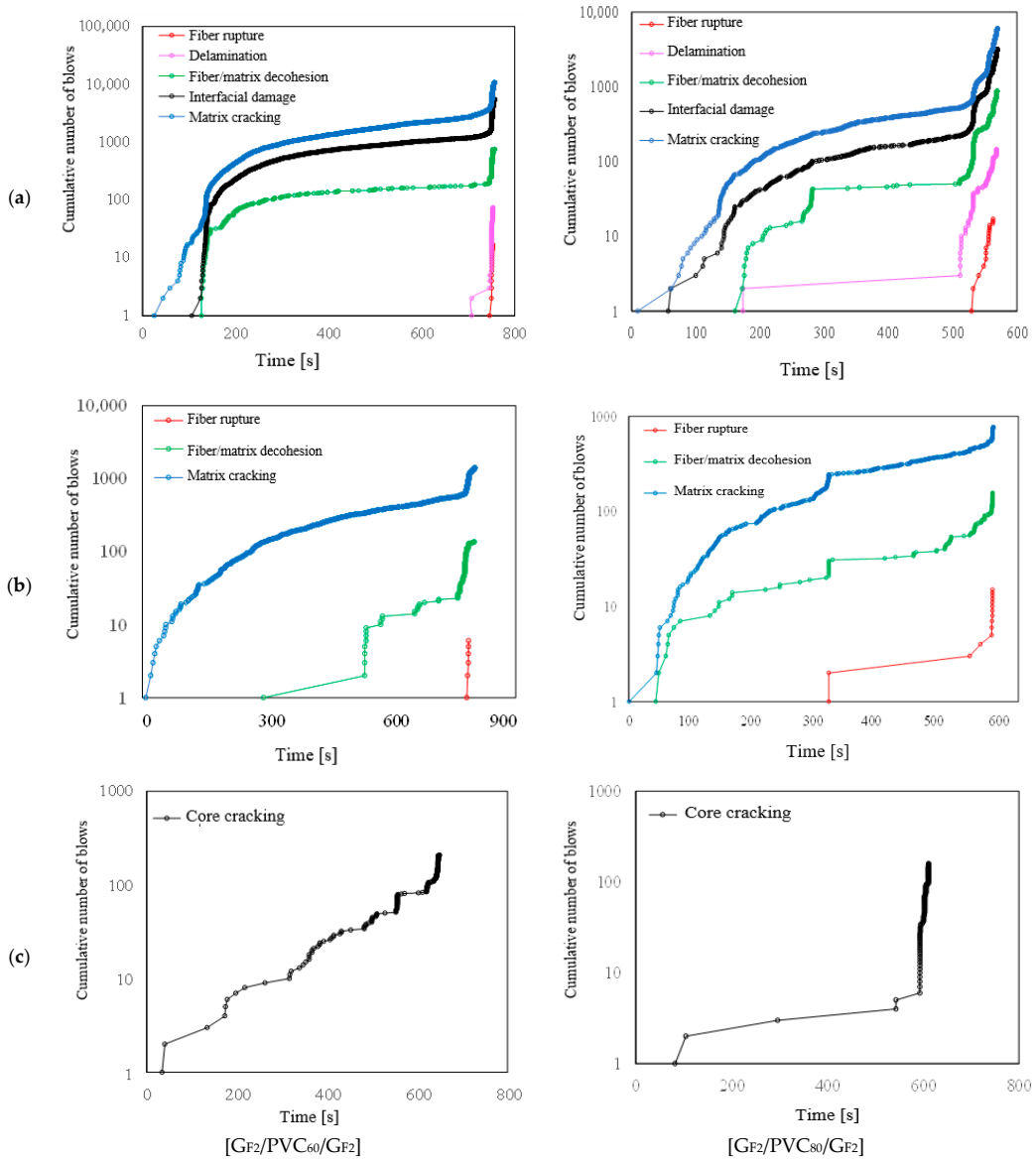

Figure 9. Acoustic emission (AE) activity recorded during bending tests on sandwich composites: (**a**) sensor attached to the top skin, (**b**) sensor attached to the bottom skin, and (**c**) sensor attached to the core.

This lack of detection is simply explained by referring to Figure 10, which shows that interfacial damage propagates only at the top interface.

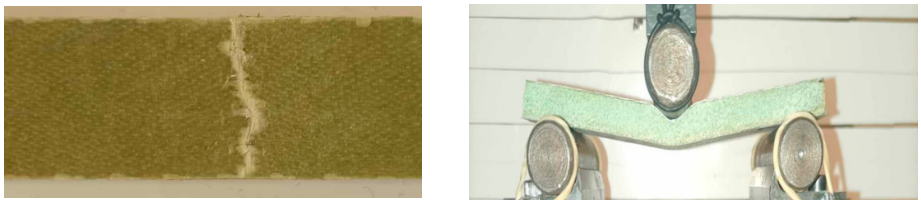

Figure 10. Typical damage modes observed on the upper surface of the sandwich composite during the bending test.

The ultimate breakdown of the sandwiches is significantly related to the breakage of the skin, particularly the upper skin, as illustrated in Figure 10. As a result, it occurs after the initiation and amplification of fiber breakdown mechanisms (0.07% in the top skin

against 0.03% in the bottom skin for [$GF_2/PVC_{60}/GF_2$], and 0.16% in the top skin versus 0.14% in the bottom skin for [$GF_2/PVC_{80}/GF_2$]). The differences in damage mechanisms discovered in the upper and lower skins are primarily due to skin type. The differences between the two core types can be related to the size of the PVC foam cells. As the density of the core increases, the size of the cells decreases, offering greater resistance, in particular, at the interface with the upper skin and greater resistance to interfacial decohesion.

Indeed, within a few seconds, the upper skin suffers its first damage: transverse cracking, which causes a local concentration of pressures at the crack ends. The second effect is the production of interlaminar cracks parallel to the fibers (delamination) in the layers as a result of matrix cracking and matrix delamination from the fibres, as illustrated in Figures 8–10, and Table 5. Transverse cracking is a gradual damaging mechanism. It builds as the applied load increases, eventually leading to layer failure, as seen in Figure 9a,b. to the global stress state induced by the specimen's bending. The central roller generates substantial localized stresses at its contact point with the core, intensifying the overall stress state induced by the specimen's bending. This effect explains the high acoustic activity detected by the sensor placed on the core, reaching up to 62 dB, as shown in Figure 9c. A Principal Component Analysis (PCA) was performed to obtain the two-dimensional visualization shown in Figure 11. The plot reveals a clear clustering of the features associated with each class. In this study, the first two principal components were retained, as they capture more than 95% of the total variance, ensuring that the reduced space preserves the key discriminative information required for the classification of the acoustic emission signals.

Table 5. Characteristics of the AE signals for each damage group in flexural sandwiches.

Waveform Characteristic	Sensor Bonded to Upper Skin		Sensor Bonded to Lower Skin		Sensor Bonded to Foam	
	Amplitude [dB]	Total Damage [%]	Amplitude [dB]	Total Damage [%]	Amplitude [dB]	Total Damage [%]
Matrix cracking 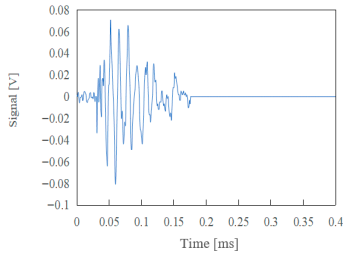	40–50	[$GF_2/PVC_{60}/GF_2$] 56.8	40–50	[$GF_2/PVC_{60}/GF_2$] 7.5	Not detected	[$GF_2/PVC_{60}/GF_2$] 0
		[$GF_2/PVC_{80}/GF_2$] 53		[$GF_2/PVC_{80}/GF_2$] 7		[$GF_2/PVC_{80}/GF_2$] 0
Fiber/matrix decohesion 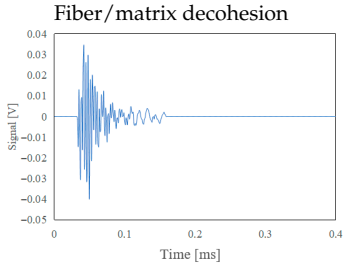	40–75	[$GF_2/PVC_{60}/GF_2$] 4.1	40–75	[$GF_2/PVC_{60}/GF_2$] 0.7	Not detected	[$GF_2/PVC_{60}/GF_2$] 0
		[$GF_2/PVC_{80}/GF_2$] 7.6		[$GF_2/PVC_{80}/GF_2$] 1.4		[$GF_2/PVC_{80}/GF_2$] 0

Table 5. *Cont.*

Waveform Characteristic	Sensor Bonded to Upper Skin		Sensor Bonded to Lower Skin		Sensor Bonded to Foam	
	Amplitude [dB]	Total Damage [%]	Amplitude [dB]	Total Damage [%]	Amplitude [dB]	Total Damage [%]
Interfacial damage 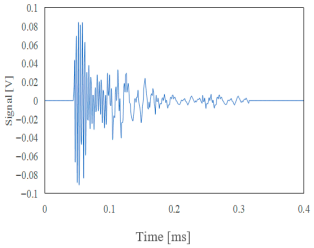	50–65	[GF_2/PVC_{60}/GF_2] 29.3 [GF_2/PVC_{80}/GF_2] 28	Not detected	[GF_2/PVC_{60}/GF_2] 0 [GF_2/PVC_{80}/GF_2] 0	Not detected	[GF_2/PVC_{60}/GF_2] 0 [GF_2/PVC_{80}/GF_2] 0
Delamination 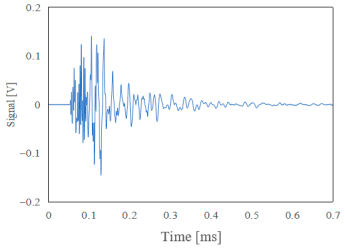	70–90	[GF_2/PVC_{60}/GF_2] 0.4 [GF_2/PVC_{80}/GF_2] 1.3	Not detected	[GF_2/PVC_{60}/GF_2] 0 [GF_2/PVC_{80}/GF_2] 0	Not detected	[GF_2/PVC_{60}/GF_2] 0 [GF_2/PVC_{80}/GF_2] 0
Fiber rupture 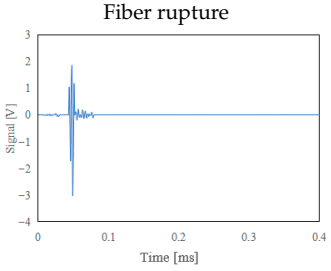	80–100	[GF_2/PVC_{60}/GF_2] 0.07 [GF_2/PVC_{80}/GF_2] 0.16	80–100	[GF_2/PVC_{60}/GF_2] 0.03 [GF_2/PVC_{80}/GF_2] 0.14	Not detected	[GF_2/PVC_{60}/GF_2] 0 [GF_2/PVC_{80}/GF_2] 0
Core cracking 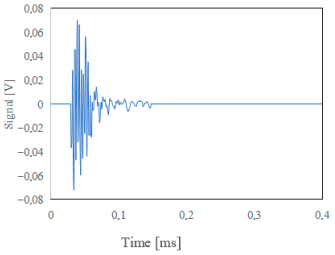	Not detected	[GF_2/PVC_{60}/GF_2] 0 [GF_2/PVC_{80}/GF_2] 0	Not detected	[GF_2/PVC_{60}/GF_2] 0 [GF_2/PVC_{80}/GF_2] 0	40–75	[GF_2/PVC_{60}/GF_2] 1.1 [GF_2/PVC_{80}/GF_2] 1.4

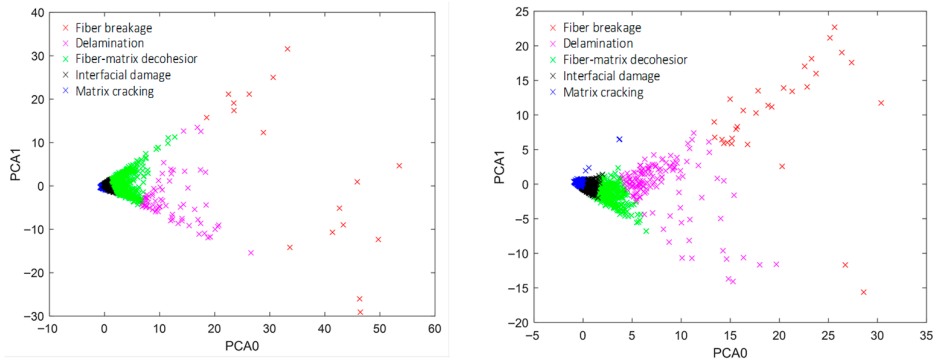

Figure 11. Visualisation of PCA of K-means clustering for static bending tests with sensors placed in the top skin (**a**) [GF2/PVC$_{60}$/GF2] and (**b**) [GF2/PVC$_{80}$/GF2].

To assess whether the identified classes correspond to distinct mechanisms, the signals from each class are initially compared with those from known damage mechanisms associated with the different components of the sandwich composite, as outlined in Table 1. Additionally, signals related to delamination and interfacial degradation between the skins and the core were identified through literature data [21,41,42]. Lastly, the overlap between the various damage mechanisms was found to be less than 15% of the total signals, consistent with the findings of Marec et al. [34].

3.2.2. Biobased Sandwich

The results of the acoustic emission associated with the evolution of the force as a function of time are given in Figure 12 for the [FF$_4$/Balsa$_{150}$/FF$_4$] sandwich.

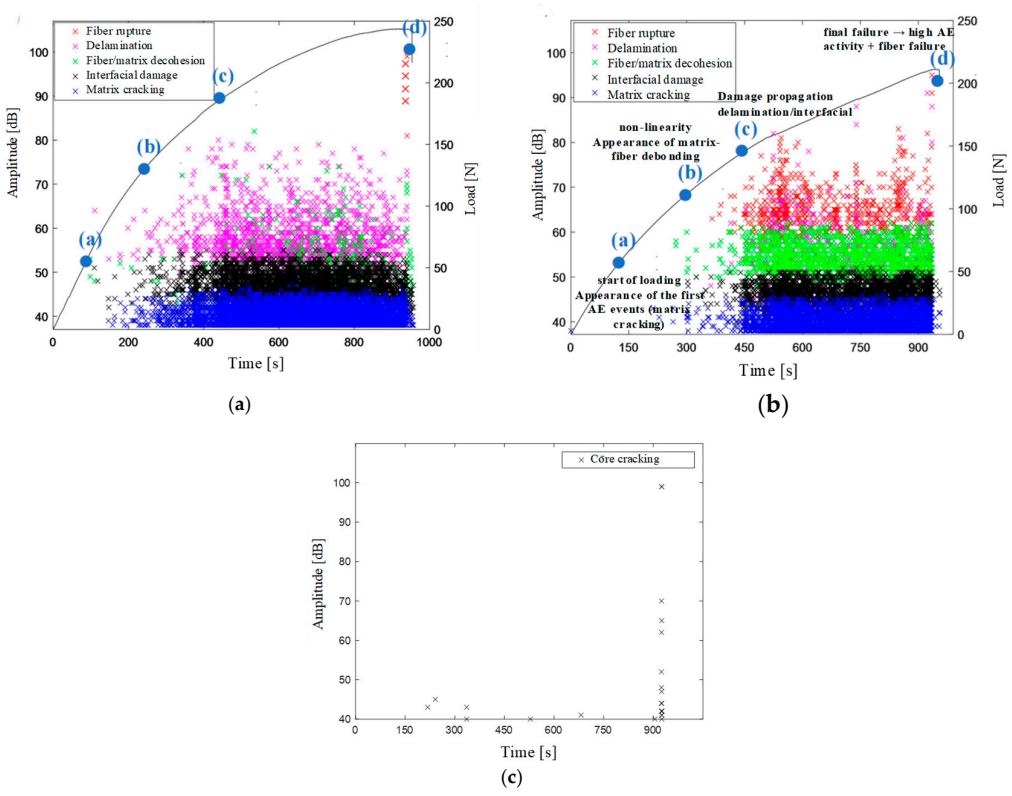

Figure 12. AE signal amplitudes over time during the flexural testing of the [FF$_4$/Balsa$_{150}$/FF$_4$] sandwich, for a sensor positioned on: (**a**) the top skin, (**b**) the bottom skin, and (**c**) the core.

Comparing the different states during static loading, Figure 13a shows the start of the test, corresponding to point (a) of the load-time curve in Figure 12. At this point, the deflection increases linearly with the load.

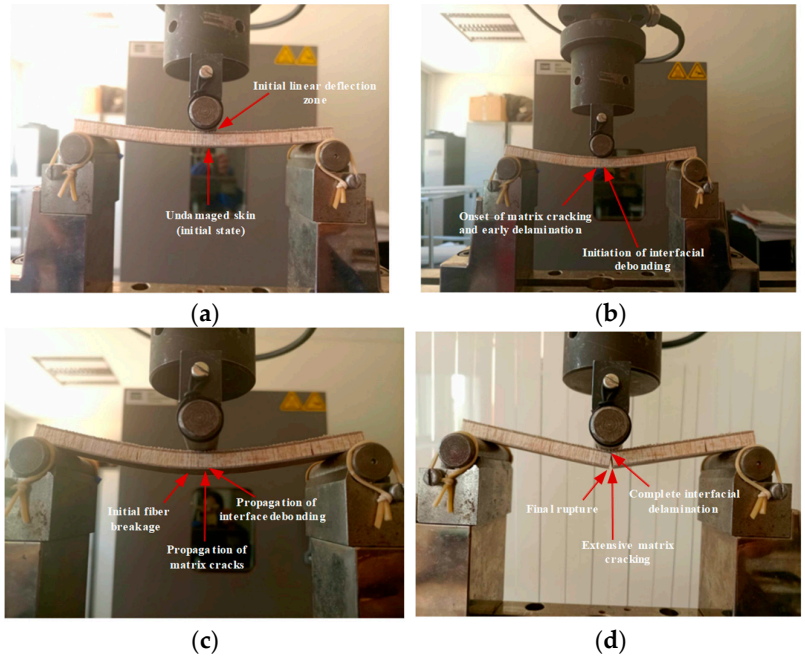

Figure 13. On-line monitoring of photographs of the balsa core beam during bending testing.

At point (b) (Figure 13b), the deflection starts to respond to the load, leading to cracks in the matrix, interfacial damage, decohesion and delamination, especially on the upper skin. The displacement curve then loses some of its linearity, and events such as fiber breakage on the lower skin and the onset of interfacial delamination between the upper skin and the core occur. These mechanisms propagate rapidly, as shown at point (c) on the load-displacement curve.

The concentrated loads caused the skin to bend more sharply, while the core absorbed much of the bending stress without fracturing. Bending of the skins continued until a limit was reached where the stresses caused the bottom skin to fracture and the sandwich sample to fail.

The final Figure 13d, taken at point (d), shows substantial damage to the sandwich. As the load increased, the interfacial debonding propagated transversely, causing the bottom skin to fail and the load to drop rapidly.

Figure 14 shows the classification results for the recorded signals. This chart depicts the progression of the number of acoustic events recorded during the bending test. According to the AE parameters shown in Table 6, the matrix cracking mechanism begins at the commencement of the bending test. It accounts for 53.65% of total injury, that is, the complete set of acoustic emission (AE) events recorded for the specimen corresponding to the sum of all identified damage mechanisms occurring in the upper skin, lower skin, and the core (43.1% in the upper skin and 10.55% in the lower skin). Quantitatively, this mechanism represents on the order of 31,000 acoustic emission events, indicating that matrix cracking contributes the largest share of the detected AE activity in these specimens.

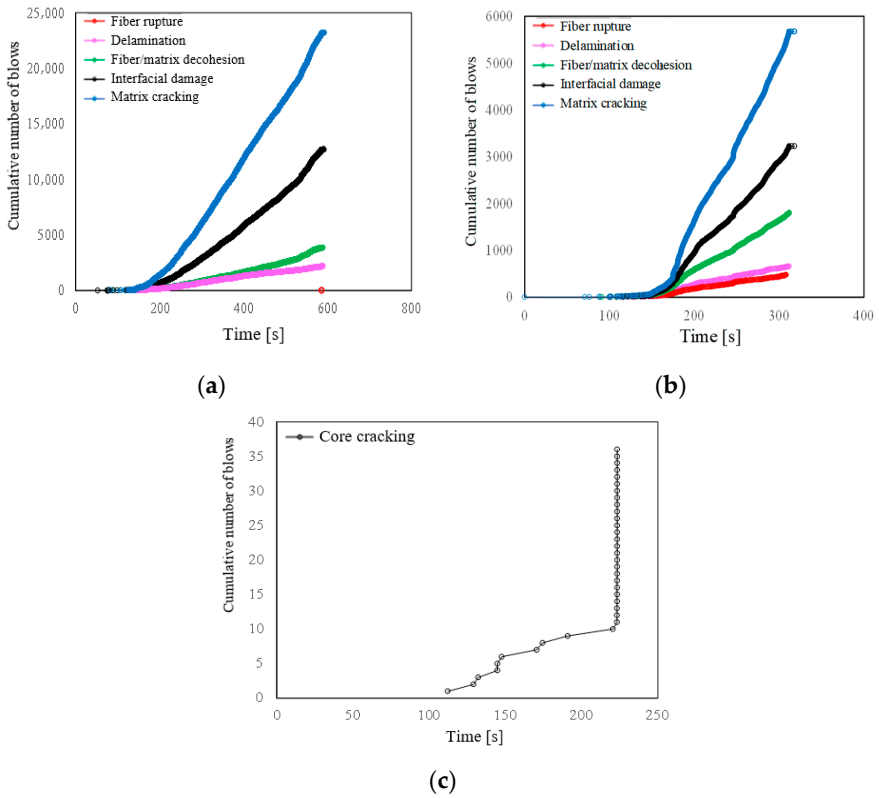

Figure 14. Chronology of occurrence and evolution of AE classes in the bio-based sandwich: (**a**) top skin, (**b**) bottom skin and (**c**) core.

This mechanism is followed by fiber/matrix decohesion (23.5% in the upper skin and 6% in the lower skin). When these two phenomena occur on both skins, delamination of the skins and interfacial delamination between the skins and the balsa core will be detected. They account for only 5.3% and 10.5% of the total damage, respectively.

It is also worth noting that the sensor placed on the balsa core records very little AE activity. This behaviour is not attributed to strong attenuation of acoustic waves in the balsa nor to inadequate sensor coupling, but rather to a real lack of significant damage within the core throughout most of the bending test. Owing to its high stiffness and excellent shear resistance, the balsa core efficiently supports and redistributes the applied stresses, delaying the onset of core cracking or interfacial degradation. As a result, the core remains largely undamaged until the bottom skin fails, after which only a limited number of core-related AE events are detected shortly before the complete collapse of the structure.

The eventual failure of the sandwich is significantly related to the failure of the skin, particularly the bottom skin, as illustrated in Figure 13d. As a result, it occurs after the commencement and acceleration of fiber failure mechanisms (0.09% in the bottom skin). The discrepancies in percentages of damage seen in the top and lower skins are primarily according to the type of core. The balsa core offers greater strength, particularly at the interface with the top skin, and greater resistance to fiber breakage.

Table 6. Characteristics of the AE signals for each damage group of the [FF_4/$Balsa_{150}$/FF_4] sandwich in flexion.

Waveform Characteristic	Amplitude [dB]	Sensor Bonded to Upper Skin	Sensor Bonded to Lower Skin	Sensor Glued to Balsa Wood
		Total Damage [%]	Total Damage [%]	Total Damage [%]
Matrix cracking 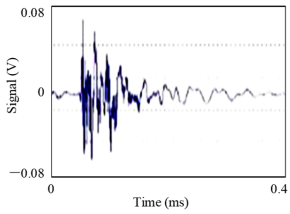	40–50	43.1	10.55	0
Fiber/matrix decohesion 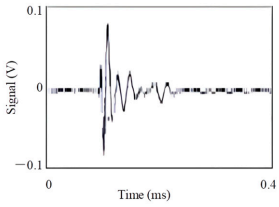	45–55	23.5	6	0
Interfacial damage 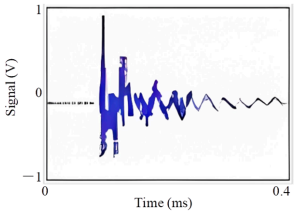	45–60	7.2	3.3	0
Delamination 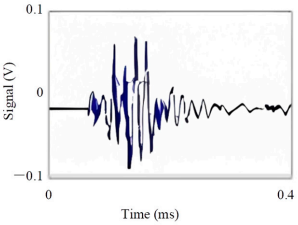	50–70	4.1	1.2	0
Fiber rupture 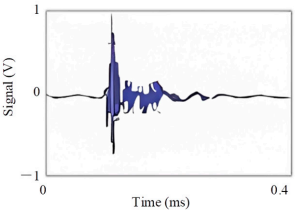	70–100	0.05	0.9	0
Core cracking 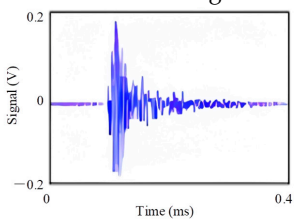	40–100	0	0	0.1

The results of previous work [24,42] are used to validate the classification of classes linked essentially to skin damage. Each of these classes has its own distinctive characteristics. The class corresponding to core cracking is distinguished by its short duration, average rise time, low absolute energy, and low amplitude [22] (less than 55 dB [25]). Similarly, the class related to interfacial damage between the skin and the core is characterised by a reduced amplitude of less than 50 dB according to Bravo et al. [25]. In order to improve the representation of the results obtained by the k-means method, a principal component analysis (PCA) was implemented. This approach reduces the complexity of the data while preserving the essential information, as shown in Figure 15.

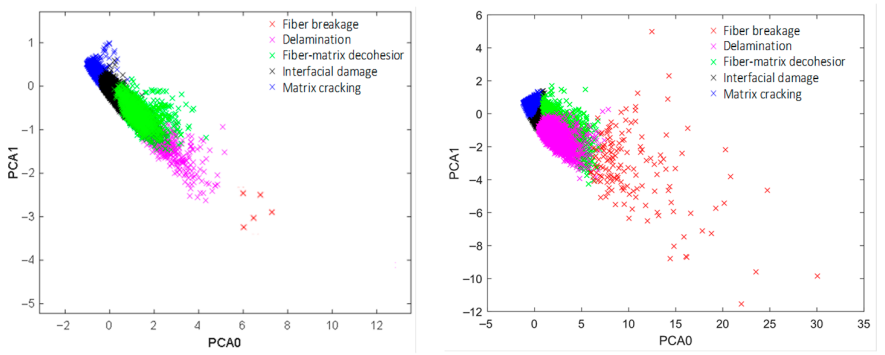

Figure 15. Visualisation of the PCA: (**a**) upper skin and (**b**) lower skin.

4. Conclusions

The aim of this work is to gain a better understanding of the damage mechanism processes in composite sandwich materials. Firstly, the elastic behavior of sandwich materials is detailed, along with a precise experimental protocol and an in-depth analysis of the behavior in bending. The determination of equivalent stiffnesses provides crucial information on the mechanical response of these complex structures. Comparative observations show that sandwiches with glass skins are stiffer than those with flax fiber skins, due to the higher modulus of the glass fabric. In addition, the results show that the [FF_4/$Balsa_{150}$/FF_4] sandwich offers better load resistance while maintaining its structural integrity, thanks to the mechanical strength of the flax and the higher density of the balsa core. Damage mechanisms were identified for the different components of the sandwich material, including the foam and skins. Through multivariate analysis of AE signals recorded during three-point bending tests, distinct acoustic signatures were attributed to each damage mechanism, such as core damage, matrix cracking, and fiber-matrix debonding. The findings indicate that matrix cracking is the predominant mechanism, occurring early in the test. Additionally, results highlight the strong dependence of AE signal detection on the positioning of piezoelectric transducers. Specifically, detecting core damage is significantly reduced when transducers are placed exclusively on the skins. Furthermore, high acoustic activity is observed when transducers are positioned on the upper skin.

In parallel, the mechanical comparison between the two categories of sandwiches reveals clear tendencies: synthetic PVC-based specimens exhibit higher bending stiffness (78–84 $N{\cdot}mm^{-1}$) than the bio-based balsa configuration (38 $N{\cdot}mm^{-1}$), whereas the latter withstands higher maximum loads (244 N versus 176–207 N) and larger breaking displacements (15.4 mm compared to 9.5–12.2 mm). From a damage perspective, PVC sandwiches are governed primarily by matrix cracking exceeding 53% of the total AE activity while the balsa sandwich, despite generating a large number of AE events on its skins, shows very little AE activity originating from the core itself, confirming that the balsa remains

largely intact during most of the test and that final failure is mainly driven by skin rupture followed by limited late-stage core degradation.

The detection of damage mechanisms could be improved by optimising the layout of the AE sensors, in particular by integrating them into the core or by adopting a wider distribution. In addition, combining AE with other non-destructive testing techniques, such as ultrasound or infrared thermography, would help to refine the identification of failure modes. Finally, the use of artificial intelligence algorithms, in particular machine learning and neural networks, would offer more reliable and automated classification of AE signals, thus improving real-time monitoring of sandwich structures.

Author Contributions: Conceptualization, H.D. and A.E.M.; methodology, H.D. and A.E.M.; software, H.D.; validation, A.E.M. and M.B. (Moez Beyaoui); formal analysis, A.E.M. and M.B. (Moez Beyaoui); investigation, M.H.; resources, H.D.; data curation, H.D.; writing—original draft preparation, H.D.; writing—review and editing, H.D.; visualization, M.B. (Mourad Bentahar); supervision, A.E.M. All authors have read and agreed to the published version of the manuscript.

Funding: This research received no external funding.

Institutional Review Board Statement: Not applicable.

Informed Consent Statement: Not applicable.

Data Availability Statement: The original contributions presented in this study are included in the article. Further inquiries can be directed to the corresponding author.

Acknowledgments: We thank the reviewers for their useful comments and feedback that help improve the manuscript.

Conflicts of Interest: The authors declare no conflicts of interest.

References

1. Zenkert, D.; Vikstrom, M. Shear cracks in foam core sandwich panels. *J. Compos. Technol. Res.* **1992**, *14*, 95–103. [CrossRef]
2. Olsson, K.A.; Lonno, A. Test procedures for foam core materials. In Proceedings of the First International Conference on Sandwich Constructions, Stockholm, Sweden, 19–22 June 1989; EMAS Ltd.: Lincoln, UK, 1989; pp. 293–318.
3. Nordstrand, T.M.; Carlsson, L.A. Evaluation of transverse shear stiffness of structural core sandwich plates. *Compos. Struct.* **1997**, *37*, 145–153. [CrossRef]
4. Daniel, M.I.; Jandro, L.A. Fabrication, testing and analysis of composite sandwich beams. *Compos. Sci. Technol.* **2000**, *60*, 2455–2463. [CrossRef]
5. Pirinu, A.; Saponaro, A.; Nobile, R.; Panella, F.W. Low-Velocity Impact Damage Quantification on Sandwich Panels by Thermographic and Ultrasonic Procedures. *Exp. Tech.* **2024**, *48*, 299–322. [CrossRef]
6. Liu, Y.; Hu, Y.; Zhang, J.; Liu, H.; Wan, M. Non-Destructive Testing of a Fiber-Web-Reinforced Polymethacrylimide Foam Sandwich Panel with Terahertz Time-Domain Spectroscopy. *Sensors* **2024**, *24*, 1715. [CrossRef]
7. Tanveer, M.; Elahi, M.U.; Jung, J.; Azad, M.M.; Khalid, S.; Kim, H.S. Recent advancements in guided ultrasonic waves for structural health monitoring of composite structures. *Appl. Sci.* **2024**, *14*, 11091. [CrossRef]
8. Unnikrishnakurup, S.; Patel, R.; Zhang, Y. Damage characterization in composite sandwich structures under flexural loading. *Int. J. Appl. Mater.* **2022**, *14*, 321–330.
9. Smolnicki, M.; Kowalski, P.; Nowak, A. Non-destructive evaluation of foam-core sandwich panels using infrared thermography. *Int. J. Appl. Mater.* **2023**, *15*, 112–120.
10. Ghazouani, M.; Ben Ammar, A.; Trabelsi, M. Acoustic emission monitoring of damage mechanisms in glass fiber composites. *Int. J. Appl. Mater.* **2023**, *15*, 201–210.
11. Driss, H.; El Mahi, A.; Bentahar, M.; Beyaoui, M.; Haddar, M. Characterization of tensile and fatigue damages in composite structures using lamb wave for improved structural health monitoring. *Int. J. Appl. Mech.* **2023**, *15*, 2350014. [CrossRef]
12. Hana, D.; Moez, B.; Zeineb, K.; Abderrahim, E.M.; Mourad, B.; Mohamed, H.; Mandal, D.D. Behavior monitoring of flax fiber reinforced composites by guided waves. *Int. J. Damage Mech.* **2024**, *34*, 598–616. [CrossRef]
13. Dahmene, F.; Yaacoubi, S.; El Mountassir, M. Acoustic emission of composites structures: Story, success, and challenges. *Phys. Procedia* **2015**, *70*, 599–603. [CrossRef]

14. Maillet, E.; Baker, C.; Morscher, G.N.; Pujar, V.V.; Lemanski, J.R. Feasibility and limitations of damage identification in composite materials using acoustic emission. *Compos. Part A* **2015**, *75*, 77–83. [CrossRef]
15. Huguet, S. Application de Classificateurs Aux Donnees D'emission Acoustique: Identification de la Signature Acoustique des Mecanismes D'endommagement Dans Les Composites à Matrice Polymere. Ph.D. Thesis, INSA de Lyon, Villeurbanne, France, 2002.
16. Bourchak, M.; Farrow, I.R.; Bond, I.P.; Rowland, C.W.; Menan, F. Acoustic emission energy as a fatigue damage parameter for CFRP composites. *Int. J. Fatigue* **2007**, *29*, 457–470. [CrossRef]
17. Gutkin, R.; Green, C.J.; Vangrattanachai, S.; Pinho, S.T.; Robinson, P.; Curtis, P.T. On acoustic emission for failure investigation in CFRP: Pattern recognition and peak frequency analyses. *Mech. Syst. Signal Process.* **2011**, *25*, 1393–1407. [CrossRef]
18. Sause, M.G.R.; Gribov, A.; Unwin, A.R.; Horn, S. Pattern recognition approach to identify natural clusters of acoustic emission signals. *Pattern Recognit. Lett.* **2012**, *33*, 17–23. [CrossRef]
19. De Groot, P.J.; Wijnen, P.A.M.; Janssen, R.B.F. Real-time frequency determination of acoustic emission for different fracture mechanisms in carbon/epoxy composites. *Compos. Sci. Technol.* **1995**, *55*, 405–412. [CrossRef]
20. Li, L.; Lomov, S.V.; Yan, X. Correlation of acoustic emission with optically observed damage in a glass/epoxy woven laminate under tensile loading. *Compos. Struct.* **2015**, *123*, 45–53. [CrossRef]
21. Yan, L.; Kasal, B.; Huang, L. A Review of Recent Research on the Use of Cellulosic Fibres. *Compos. Part B Eng.* **2016**, *92*, 94–132. [CrossRef]
22. Mehdaoui, I.; Haldhar, R.; Arrousse, N.; Al-Zaqri, N.; Hassani, E.S.; Hajjaji, F.E.; Taleb, M.; Rais, Z.; Kim, S.-C. Surface treatment and corrosion protection of mild steel by the oily extracts of olive mill waste cake. *J. Appl. Electrochem.* **2023**, *53*, 1505–1518. [CrossRef]
23. Kersani, M.; Lomov, S.V.; Van Vuure, A.W.; Bouabdallah, A.; Verpoest, I. Damage in flax epoxy quasi unidirectional woven laminates under quasi-static tension. *J. Compos. Mater.* **2015**, *49*, 403–413. [CrossRef]
24. Rhomany, G.; Karger-Kocsis, J.; Czigany, T. Tensile fracture and failure behavior of technical flax fibers. *J. Appl. Polym. Sci.* **2003**, *90*, 3638–3645. [CrossRef]
25. Bravo, A.; Toubal, L.; Koffi, D.; Erchiqui, F. Characterization of Tensile Damage for a Short Birch Fiber-reinforced Polyethylene Composite with Acoustic Emission. *Int. J. Mater. Sci.* **2013**, *3*, 79–89.
26. Monti, A. Elaboration et Caracterisation Mecanique D'une Structure Composite Sandwiche à Base de Constituants Naturels. Ph.D. Thesis, Le Mans Université, Le Mans, France, 2016.
27. Wang, Y.; Yang, S.; Luo, Q.; Li, Q.; Sun, G. Experimental characterization of impact damage in foam-core sandwich structures using acoustic emission, optical scanning, and X-ray computed tomography. *Compos. Part B* **2023**, *240*, 110919. [CrossRef]
28. Kucukkalfa, E.; Ghaderiaram, A.; Yildiz, K.; Fotouhi, M.; Asadi, A.; Cebeci, H. Damage detection of CNT/CNC-reinforced foam-cored sandwich composites by acoustic emission tests under flexural load. *Compos. Struct.* **2023**, *314*, 116964.
29. Wu, Y.; Perrin, M.; Pastor, M.L.; Casari, P.; Gong, X. Moisture effects on acoustic emission characteristics and damage mechanisms of balsa wood core composite sandwich under 4-point bending. *Materials* **2024**, *17*, 1044. [CrossRef]
30. Pyrzowski, Ł.; Knak, M.; Rucka, M. Failure characterisation of sandwich beams using integrated acoustic emission and digital image correlation techniques. *Compos. Struct.* **2023**, *322*, 117361. [CrossRef]
31. Yahyaoui, I. Contribution au Suivi par Emission Acoustique de L'endommagement des Structures Multi-Matériaux à Base de Bois. Ph.D. Thesis, Université Toulouse III-Paul Sabatier, Toulouse, France, 2017.
32. Assarar, M.; Bentahar, M.; El Mahi, A.; El Guerjouma, R. Monitoring of damage mechanisms in sandwich composite materials using acoustic emission. *Int. J. Damage Mech.* **2015**, *24*, 787–804. [CrossRef]
33. Roundi, W.; El Mahi, A.; Rebiere, J.L.; El Gharad, A. Monitoring damage evolution with acoustic emission in two types of glass epoxy laminates. *Polym. Polym. Compos.* **2022**, *30*, 09673911221109906. [CrossRef]
34. Chen, O.; Karandikar, P.; Takeda, N.; Rcast, T.K. Acoustic emission characterization of a glass-matrix composite. *Nondestruct. Test. Eval.* **1992**, *8*, 869–878. [CrossRef]
35. Hamdi, S.E.; El Guerjouma, R.; Ben Ghozlen, M.H. Analyse des mécanismes d'endommagement par émission acoustique des matériaux composites utilisant la méthode de l'implant piézoélectrique. In Proceedings of the 5th International Conference Sciences of Electronic, Technologies of Information and Telecommunications, Hammamet, Tunisia, 22–26 March 2009.
36. Ben Ameur, M.; El Mahi, A.; Rebiere, J.-L.; Gimenez, I.; Beyaoui, M.; Abdennadher, M.; Haddar, M. Investigation and identification of damage mechanisms of unidirectional carbon/flax hybrid composites using acoustic emission. *Eng. Fract. Mech.* **2019**, *216*, 106511. [CrossRef]
37. *NF T 54-606*; Plastics Based Sandwich Structures — Bend Test. AFNOR: La Plaine Saint-Denis, France, October 1987.
38. Likas, A.; Classis, N.J.; Verbeek, J. The global k-mean clustering algorithm. *Pattern Recognit. Lett.* **2003**, *36*, 451–461. [CrossRef]
39. Milligan, G.W.; Cooper, M.C. An examination of procedures for determining the number of clusters in a data set. *Psychometrika* **1985**, *50*, 159–179. [CrossRef]

40. Roundi, W.; El Mahi, A.; El Gharad, A.; Rebière, J.-L. Experimental and numerical investigation of the effects of stacking sequence on the mechanical behavior of hybrid composite materials. *Compos. Struct.* **2018**, *200*, 776–791.
41. Marec, A.; Thomas, J.-H.; El Guerjouma, R. Damage characterization of polymer-based composite materials: Multivariable analysis and wavelet transform for clustering acoustic emission data. *Mech. Syst. Signal Process.* **2008**, *22*, 1441–1464. [CrossRef]
42. El Mahi, A.; Ben Salem, I.; Assarar, M.; Berbaoui, R.; Poilane, C.; El Guerjouma, R. Analyse par émission acoustique de l'endommagement des matériaux éco-composites. In Proceedings of the 10ème Congrès Français d'Acoustique, Lyon, France, 12–16 April 2010.

Disclaimer/Publisher's Note: The statements, opinions and data contained in all publications are solely those of the individual author(s) and contributor(s) and not of MDPI and/or the editor(s). MDPI and/or the editor(s) disclaim responsibility for any injury to people or property resulting from any ideas, methods, instructions or products referred to in the content.